International Journal of Thermofluids 21 (2024) 100547

Contents lists available at ScienceDirect

International Journal of Thermofluids

journal homepage: www.sciencedirect.com/journal/international-journal-of-thermofluids

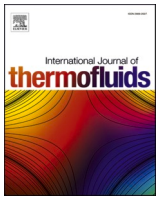

# Novel Unscented Kalman Filter-based method to assess the thermal behavior of carbon brake discs for high-performance motorcycles

Federico Bonini [a], Alessandro Rivola [a,b], Alberto Martini [a,b,*]

[a] DIN-Department of Industrial Engineering, University of Bologna, V.le del Risorgimento 2, Bologna, BO 40136, Italy
[b] CIRI-MAM, Advanced Applications in Mechanical Engineering and Materials Technology, University of Bologna, V.le del Risorgimento 2, Bologna, BO 40136, Italy

ARTICLE INFO

*Keywords:*
Bayesian filter
Unscented Kalman Filter
Parameter identification
State estimation
Finite element thermal model

ABSTRACT

In the past few decades, braking systems with carbon discs have become the dominant technology for many racing applications, such as in the MotoGP class. Indeed, they provide higher friction coefficients. Moreover, thanks to their lightweight materials (with respect to conventional steel brakes), the unsprung masses and the gyroscopic effects can be reduced. Therefore, the motorcycle dynamic performance can be significantly improved. The usage of carbon brakes requires a very accurate assessment of their thermal behavior. In fact, although their operating temperature in real racing conditions may cover a wide range, their optimal braking performance can be achieved only within a relatively narrow temperature range. This work focuses on the development of the Unscented Kalman Filter (UKF) algorithm as a suitable mathematical tool for assessing the temperature gradient of the carbon disc mounted on the motorcycles competing in the MotoGP™ world championship. A one-dimensional (1D) finite element (FE) model of the disc is developed to provide the a priori state estimate that the filter will combine with the information measured by the temperature sensor available on board to compute the optimal posterior temperature estimation. Besides estimating temperature, the UKF is also exploited to identify the convection heat transfer coefficient ($h$) of the disc, which is a fundamental parameter for a proper model calibration.

## 1. Introduction

Carbon-based materials can provide to braking systems a combination of light weight, high thermal conductivity and absence of thermal expansion, which is currently hard to achieve with other materials [1]. These characteristics result in a high friction coefficient, stable and consistent braking effectiveness, and very high heat dissipation. Given the higher braking capabilities with respect to the conventional steel brakes, carbon brakes are adopted for high-performance applications, such as aircraft landing gears, as well as racing cars and motorcycles. Indeed, carbon-carbon brakes have become the absolute standard in the MotoGP™ world championship. The carbon-carbon composite presents both the matrix and the reinforcing fibers made out of carbon, hence being usually referred as C/C brakes.

Whether conventional steel brakes or C/C brakes are adopted, the knowledge of the working temperature range at which the disc will operate is fundamental to predict the performance in terms of friction coefficient [2], wear [3], thermal deformation and brake fluid vaporization [4], and therefore to properly design braking systems as well [5]. The Company that supplies the braking systems of the MotoGP™ motorcycles published in a work by Cividini et al. [6] the latest findings concerning design methods, simulation procedures, product features and manufacturing processes of C/C racing brakes. This study highlights how the disc temperature control is fundamental not only for the good performance and repeatability of the overall braking system but also for the tire temperature control. In fact, due to their position on the vehicle, brakes are often employed as a way to better control tire temperature in racing application, further contributing to the overall vehicle performance.

MotoGP motorcycles are equipped with an infrared transducer (referred to as *single-spot* sensor hereafter) that detects the disc temperature at a fixed radial distance where the disc-pads contact occurs. However, the temperature measured by the single-spot sensor, besides being quite noisy, is not representative of the thermal dynamics of the braking system, since the disc surface exhibits a high temperature gradient. Therefore, additional tools to accurately estimate the transient thermal behavior of the disc would be beneficial to assess the actual motorcycle braking performance.

Different solutions can be found in the literature to evaluate the

* Corresponding author at: DIN-Department of Industrial Engineering, University of Bologna, V.le del Risorgimento 2, Bologna, BO 40136, Italy.
*E-mail address:* alberto.martini6@unibo.it (A. Martini).

https://doi.org/10.1016/j.ijft.2023.100547

Available online 13 December 2023

**Nomenclature**

*Abbreviations*

| | |
|---|---|
| C/C | Carbon – carbon |
| CFD | Computational fluid dynamics |
| EKF | Extended Kalman Filter |
| Exp | Experimental data |
| FE | Finite Element |
| FWTD | friction and wear thermal dynamics method |
| HDF | heat dynamics of friction |
| IMU | Inertial measurement unit |
| KF | Kalman Filter |
| NDA | Non disclosure agreement |
| PDE | Partial differential equation |
| PF | Particle filter |
| RMSE | Root mean square error |
| UKF | Unscented Kalman Filter |
| 1D | One-dimensional |
| 2D | Two-dimensional |
| 3D | Three-dimensional |

*Symbol*

| | |
|---|---|
| $\mathbf{A}_{\text{cond}}$ | Conduction matrix |
| $\mathbf{A}_{\text{conv}}$ | Convection matrix |
| $\mathbf{A}_{k-1}$ | Dynamic model matrix at time step *k-1* |
| $c_v$ | Specific heat $\left[\frac{\text{J}}{\text{kg K}}\right]$ |
| $\mathbf{C}_k$ | Cross-covariance matrix in a non-linear Kalman filter at time step *k* |
| $dr$ | Infinitesimal width [*m*] |
| $e_{k-1}$ | Gaussian process noise variance at time step *k-1* |
| $f(r)$ | Specific power $\left[\frac{W}{m^2}\right]$ |
| $\mathbf{f}_{k-1}$ | Dynamic model function at time step *k-1* |
| $g(r,t)$ | Heat source function per unit volume $\left[\frac{\text{W}}{m^3}\right]$ |
| $\mathbf{g}_k$ | Measurement model function at time step *k* |
| $h$ | Convection heat transfer coefficient $[\frac{W}{Km^2}]$ |
| $h_{ref}$ | Reference convection heat transfer coefficient $[\frac{W}{Km^2}]$ |
| $\mathbf{H}_{k-1}$ | Measurement model matrix at time step *k-1* |
| $K_c$ | Thermal conductivity $\left[\frac{\text{W}}{\text{Km}}\right]$ |
| $k$ | Time step number |
| $\mathbf{K}_k$ | Kalman gain matrix at time step *k* |
| $l(r)$ | Initial temperature distribution on the disc [K] |
| $\mathbf{m}_k$ | Predicted mean of a Kalman Gaussian filter at time step *k* |
| $\mathbf{m}_k^-$ | Predicted mean of a Kalman Gaussian filter at time step *k* just before the measurement $y_k$ |
| $\mathbf{M}$ | Heat capacity matrix |
| $n$ | Positive integer referring to the dimensionality of the state |
| $\mathbf{p}$ | Thermal force matrix |
| $\mathbf{P}_k$ | Predicted state covariance matrix of a Kalman Gaussian filter at time step *k* |
| $\mathbf{P}_k^-$ | Predicted state covariance matrix of a Kalman Gaussian filter at time step *k* just before the measurement $y_k$ |
| $\mathbf{q}_{k-1}$ | Gaussian process noise at time step *k-1* |
| $\dot{Q}_{BRK}$ | Total instantaneous braking power [W] |
| $\dot{Q}_{con}$ | Rate of heat flow dissipated by convection [W] |
| $\dot{Q}_{fr}$ | Rate of heat flow generated with the pads [W] |
| $\dot{Q}_{in}$ | Rate of heat flow [W] |
| $\mathbf{Q}_{k-1}$ | Process noise covariance matrix at time step *k-1* |
| $\dot{Q}_{out}$ | Rate of heat flow [W] |
| $\dot{Q}_{rad}$ | Rate of heat flow dissipated by radiation [W] |
| $r$ | Generic radius [m] |
| $r_{\text{est}}$ | Disc external radius [m] |
| $r_{\text{int}}$ | Disc internal radius [m] |
| $\mathbf{r}_k$ | Gaussian measurement noise at time step *k* |
| $\mathbf{R}_k$ | Output (measurement) covariance matrix at time step *k* |
| $\mathbb{R}_{\text{n}}$ | n-dimensional space of real numbers |
| s | Thickness [*m*] |
| $\mathbf{S}_k$ | Innovation covariance of a Kalman/Gaussian filter at time step *k* |
| $T(r,\ t)$ | Disc temperature [K] |
| $T_{amb}$ | Environmental temperature [K] |
| $T_{\text{node-i}}$ | Time dependent nodal temperature [K] |
| $T_{ref}$ | Reference temperature [K] |
| $U$ | Internal energy [*J*] |
| $Vx$ | Longitudinal velocity $\left[\frac{m}{s}\right]$ |
| $Vx_{ref}$ | Reference longitudinal velocity $\left[\frac{m}{s}\right]$ |
| $W_i^{(c)}$ | Covariance weight of the unscented transform |
| $W_i^{(m)}$ | Mean weight of the unscented transform |
| $\mathbf{x}_k$ | State at the time at time step *k* [K] |
| $\chi_{k-1}^{(i)}$ | *i*-th sigma point of the state $\mathbf{x}_k$ |
| $\widehat{\chi}_k^{(i)}$ | *i*-th predicted sigma point of the state $\mathbf{x}_k$ |
| $\chi_k^{-(i)}$ | *i*-th sigma point of the predicted state $\mathbf{x}_k$ |
| $y_k$ | Measurement at time step *k* [K] |
| $\mathbf{y}_{1:k}$ | Set containing the measurement vectors $\{\mathbf{y}_1,\ldots,\ \mathbf{y}_k\}$ [K] |
| $\widehat{Y}_k^{(i)}$ | *i*-th predicted sigma point of the measurement $y_k$ |
| $z_k$ | Normalization constant |
| $\mathbf{z}_{k-1}$ | Combined state and parameter dynamic model function |

*Greek symbol*

| | |
|---|---|
| $\Delta t$ | Time step of each iteration [*s*] |
| $\varepsilon$ | Emissivity [-] |
| $\varepsilon_{k-1}$ | Gaussian process noise at time step *k-1* $[\frac{W}{Km^2}]$ |
| $\lambda$ | Parameter of the unscented transform |
| $\boldsymbol{\mu}_k$ | Predicted mean of measurement $y_k$ in a Kalman/Gaussian filter at time step *k* |
| $\rho$ | Material density $[\frac{kg}{m^3}]$ |
| $\sigma$ | Stefan-Boltzman constant $[\frac{W}{K^4m^2}]$ |

*Notational Convention*

| | |
|---|---|
| $N(\cdot)$ | Gaussian distribution |
| $p(x\|y)$ | Conditional probability of x given y |

temperature distribution of brake rotors. The majority of works investigating the thermal dynamics of braking systems deals with conventional (i.e. steel or cast iron) rotors, which accounts for almost 70 % of applications [1]. Yevtushenko et al. [7] proposed an analytical model to estimate the non-stationary temperature of brake disc and pads, and performed numerical analyses for a cast-iron disc in two cases, namely constant velocity sliding and constant deceleration. Sheridan et al. [8] proposed four different models for conventional rotors, namely a lumped parameter model, a one-dimensional (1D) analytical model, a two-dimensional (2D) finite difference model and an three-dimensional (3D) finite element (FE) model. The latter was solved in NASTRAN (and validated on a test rig with simulated braking sequence) to find the transient disc temperature distribution. Yevtushenko et al. [9] investigated numerically the thermal sensitivity of the frictional heating during braking for a steel disc, by means of 1D-FE model of the thermal problem. Talati et al. [10] studied the conduction heat flow of a ventilated steel brake disc for cars through numerical simulation with a 2D-FE model. Grzes [11] simulated the temperature distribution of a steel rotor during an emergency braking maneuver by means of a 2D-FE model. McPhee et al. [12] characterized the convective heat transfer

of vented cast-iron brake discs through experimental measurements on a test bench simulating the cooling phase. In general, some simplifying assumptions have been considered for both simulations and tests, e.g. single braking maneuvers, constant pressure, or constant deceleration. Moreover, model validation has been typically performed through experimental measurements on test rigs.

Only few papers dealing with the temperature estimation of C/C brakes are available. Chichinadze [13] investigated the possible use of a previously developed method, referred to as friction and wear thermal dynamics method (FWTD), as an analytical tool to assess the operation of tribological couples, possibly including multi-disc aircraft brakes. Guo et al. [14] developed a 3D-FE model to perform the thermoelastic analysis (namely predicting the coefficients of thermal expansion and thermal conductivity) of needled C/C composites in multi-disc aircraft brakes. Yevtushenko et al. [15] formulated a 2D heat dynamics of friction (HDF) system of equations to determine the operational characteristics of a multi-disc aircraft brake. The problem is solved numerically by using the FE approach. Meunier et al. [16] established a 1D numerical model of a multi-disc aircraft carbon brake to evaluate the heat flux exchanged inside the wheel and brake assembly during braking and cooling phases. In the proposed model, the heat transfer is supposed to be unidirectional in the transverse (i.e. axial) direction and homogeneous on the radial axis. It's worth noting that all the mentioned works take into account aircraft brakes, whose main characteristics (typically, multiple rotors and stators engaging along a shared rotational axis, and thermal behavior more influenced by the brake overall thickness than by the disc radius) significantly differ from the ones of motorcycle braking systems. To the Authors' best knowledge, no works dealing with the thermal behavior of motorcycle C/C brakes can be found in the literature.

This study aims at developing numerical tools to estimate the instantaneous surface temperature distribution in the C/C front brake discs of a MotoGP motorcycle in real operating conditions, by using as inputs the telemetry signals collected during test sessions with several consecutive laps. Having a fast and accurate prediction of the actual brake thermal behavior before the race may allow to better assess the braking performance in terms of available torque (by evaluating the average disc temperature in the disc/pads contact region that determine the actual friction coefficient) and to calculate the heat radiated to the front tire (that affects grip and wear), hence permitting to optimize the motorcycle configuration for the race. The desired tools are not required to run in real-time. Indeed, telemetry data are not available in real-time, but must be downloaded from an on-board datalogger when the motorcycle comes back to the box after a test session. Nonetheless, a low computational time is mandatory, in order to leave enough time for possible modifications in the motorcycle mechanical setup. Accordingly, the desired algorithm for temperature estimation should take about 5 min for processing all the laps of a race. Moreover, it must be implemented in Matlab environment, in order to be integrated with the other existing tools currently adopted for analyzing the telemetry data.

The thickness of a MotoGP C/C front brake disc is very small with respect to its diameter (maximum thickness 8 mm, maximum diameter 355 mm). Therefore, to possibly achieve a trade-off between high accuracy and low computational complexity, the temperature gradient along the disc thickness is considered negligible as a first tentative assumption, and the most relevant heat transfer direction is considered the radial axis. Accordingly, a 1D-FE thermal model of the disc with uniform power distribution in the disc/pads contact region is developed. Given the initial temperature of the brake, the instantaneous braking power, the speed of the vehicle and the environmental temperature, the FE model is able to predict the disc surface temperature as a function of the disc radial position and time. However, during the race, the actual disc temperature may be affected by many external factors that such a simplified model can not take into account, e.g. the presence of a slip stream (generated by a preceding motorcycle), and non-uniform pressure distribution in the caliper or pads wearing. In all this cases, the actual temperature of the disc may drift away from the simulated results. Hence, in light of the limitations of the simplified 1D-FE model, as well as of the single-spot sensor measurements, implementing a state observer to increase the accuracy in the disc temperature prediction is deemed convenient.

Kalman Filters (KF) are probably the most widespread algorithms among the model-based observers, since they permit to manage both measurement noise and model approximations. Indeed, many automotive applications involving the estimation of different kinematic and dynamic quantities through KF can be found in literature. Romualdi et al. [17] achieved a real-time estimation of the roll angle of a motorcycle by exploiting an Extended Kalman Filter (EKF) and the signals of the vehicle Inertial Measuring Unit (IMU). Teerhuis et al. [18] proposed a state estimator of the motorcycle lateral dynamics based on a simplified analytical model and an EKF. Dakhlallah et al. [19] estimated the sideslip angle and the tire/road interactions of a four-wheeled vehicle through an EKF. Bogdanski et al. [20] evaluated the use of EKF, Unscented Kalman Filter (UKF) and Particle Filter (PF) as possible solutions to estimate different state variables of four-wheeled vehicles. Martinez et al. [21] presented a very interesting approach, where the temperature predicted with a simple lumped parameter model is corrected using an Extended Kalman filter (EKF) and the available wheel speed measurements. However, to the authors' best knowledge, the use of state observers for C/C braking systems, and specifically for assessing the temperature distribution of brake discs, has not been investigated.

In this work, a UKF is identified as the most convenient observer to be combined with the developed thermal model and the available measurements. Firstly, a UKF is implemented and exploited to identify the convection coefficient of the disc, which is fundamental for a proper calibration of the 1D-FE model. Then, the UKF formulation is slightly modified to yield the posterior optimal temperature estimation, by updating the theoretical temperature prediction performed by the FE model with the empirical information coming from the single-spot temperature transducer. The developed approach is expected to be sufficiently accurate and robust, and to meet the computational efficiency requirements.

The main merits of the paper can be summarized as follows. In the first place, the thermal behavior of C/C brakes for motorcycles is studied, which is a topic apparently not covered by the literature. In the second place, a UKF is combined with a simple 1D-FE model to achieve a fast and effective tool to estimate the actual temperature distribution of the C/C disc. Finally, the UKF-based algorithm is used also to identify the actual convection heat transfer coefficient, to refine the 1D-FE model and the final estimation accuracy. The proposed approach (in particular the use of a UKF for both parameter identification and state estimation) to achieve the dynamic thermal assessment of a braking system has not been investigated previously.

The paper is structured as follows. In Section 2, the experimental data available for the study are described. Section 3 goes through the development of the finite element model of the disc. The UKF implementation is presented in Section 4. Both the UKF architectures used for the convection coefficient identification and for temperature estimation are discussed. The main results provided by the developed algorithm are reported in Section 5. Finally, the conclusions are drawn in Section 6.

## 2. Experimental tests

A collaboration with Ducati Corse (a division of Ducati Motor Holding S.p.A., Bologna, Italy) was successfully started, allowing to conduct this research activity using real data and testing the new methodologies more effectively. The dataset was acquired performing some track tests in which the single-spot transducer regularly available on the front disc was replaced with a multi-spot sensor able to measure the disc temperature in four different radial positions, as shown in Fig. 1. It is important to note that the third spot of the multi-spot sensor, referred to as *Spot3*, coincides with the position of the single-spot sensor

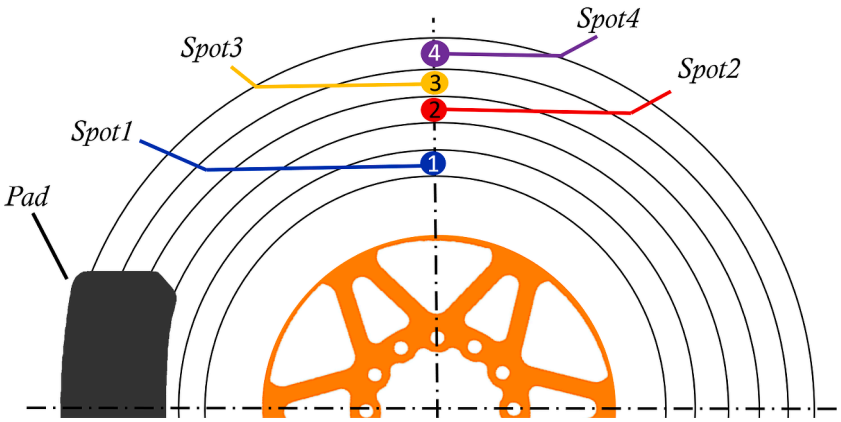


**Fig 1.** Schematic of the multi-spot temperature sensor setup.

mounted during the race.

The specifications of the C/C discs employed during tests, which can be disclosed in compliance with the NDA, are reported in Table 1.

The introduction of the multi-spot sensor revealed that the three spots placed on the contact patch between the pads and the disc (*Spot2-4*) do not always share similar temperature values (Fig. 2). Indeed, large gradients can be generated in the most aggressive braking maneuvers, hence the single-spot temperature acquisition being not representative of the actual thermal behavior of the system. For instance, it can be observed, for time equal to about 90 s, that the temperature in the central region of the contact patch (*Spot3*) can reach a temperature remarkably higher than in the adjacent regions (*Spot2* and *Spot4*). Reasonably, the observed behavior is ascribable to the combination of a non-uniform pressure distribution in the brake caliper and a non-uniform wear of the braking pads. However, a repeatable pattern associated to the peak amplitudes can not be identified: the disc temperature distribution can drastically change not only from corner to corner but also for the same braking maneuver in consecutive laps. As a consequence, both these phenomena can not be taken into account by the thermal model, and the power dissipated during braking is initially assumed to be distributed uniformly along the whole contact patch. Normalized results are reported in this chart and hereafter, due to NDA. In particular, the normalized temperature is obtained by dividing the actual disc temperature, $T$, by a reference value, $T_{ref}$.

The UKF is firstly employed to estimate the convection coefficient of the brake, by exploiting all the four temperature measurements. Once this parameter is identified, a law for the variation of $h$ with respect to the forward velocity of the vehicle is implemented in the FE model interpolating the values estimated previously by the UKF. Subsequently the actual temperature gradient measured by the multi-spot sensor is used to validate both the fully calibrated FE model and the UKF algorithm. In this phase the UKF architecture was modified so that it estimates only the temperature distribution on the disc using the measurements of the third spot, simulating the actual input condition available during races. The other measurements (i.e. *Spot1, Spot2* and *Spot4)* are used for validation purposes only. It is important to remember that the multi-spot sensor is not allowed during races and the final goal is achieving an offline estimate of the temperature distribution based on the onboard (single-spot) sensor measurements. In addition to the temperature values, the signals regarding the forward speed of the vehicle, the angular velocity of the front wheel and the fluid pressure in the braking circuit are acquired and fed to the FE model as inputs. Every telemetry signal is filtered and downsampled to 10 Hz in order to reduce the algorithm execution time.

**Table 1**
Main specifications of the tested C/C discs.

| Parameter | Value |
|---|---|
| External radius ($r_{est}$) | 0.340 [m] |
| Thickness ($s$) | 0.008 [m] |
| Mass ($m_{tot}$) | ≈ 1.000 [kg] |
| Nominal lower operating temperature | 250 [°C] |
| Nominal upper operating temperature | 850 [°C] |

## 3. One-dimensional finite element model

Before building the FE model it is necessary to derive the local governing equation that describes the heat exchange in the disc. For this purpose, a generic infinitesimal ring of radius $r$ and width $dr$ is considered, as shown in Fig. 3: its temperature can be approximated as uniform throughout its whole volume. Note that since the model is 1D, the infinitesimal ring presents the same thickness, $s$, of the original brake disc. In this way, temperature changes only along the disc radius and it is uniform in the other two directions. Fig. 3 reports the ways heat is transferred in the reference volume. $\dot{Q}_{out}$ and $\dot{Q}_{in}$ represent the rate of heat flow that flows by conduction to, respectively, the outer and from the inner part of the disc:

$$\dot{Q}_{in} = -2\pi rs \cdot K_c \cdot \frac{\partial T}{\partial r}(r) \tag{1}$$

$$\dot{Q}_{out} = -2\pi (r+dr)s \cdot K_c \cdot \frac{\partial T}{\partial r}(r+dr) \tag{2}$$

where $K_c$ is the thermal conductivity. $\dot{Q}_{con}$ and $\dot{Q}_{rad}$ represent, respectively, the rate of heat flow dissipated by convection and radiation:

$$\dot{Q}_{con} = 2 \cdot 2\pi rdr \cdot h \cdot (T - T_{amb}) \tag{3}$$

$$\dot{Q}_{rad} = 2 \cdot 2\pi rdr \cdot \sigma \cdot \varepsilon \cdot \left(T^4 - T_{amb}^4\right) \tag{4}$$

where $h$ is the convection heat transfer coefficient, $T_{amb}$ is the environmental temperature, σ is the Stefan-Boltzman constant, ε is the emissivity, and scalar 2 is for accounting both sides of the disc. Since temperature is considered uniform throughout the ring circumference and thickness, there is no heat conduction along these directions. Finally, $\dot{Q}_{fr}$ is the rate of heat flow generated by the friction with the pads,

$$\dot{Q}_{fr} = 2 \cdot 2\pi rdr \cdot f(r) \tag{5}$$

where $f(r)$ is the friction power distribution on the disc contact region, which can be expressed as

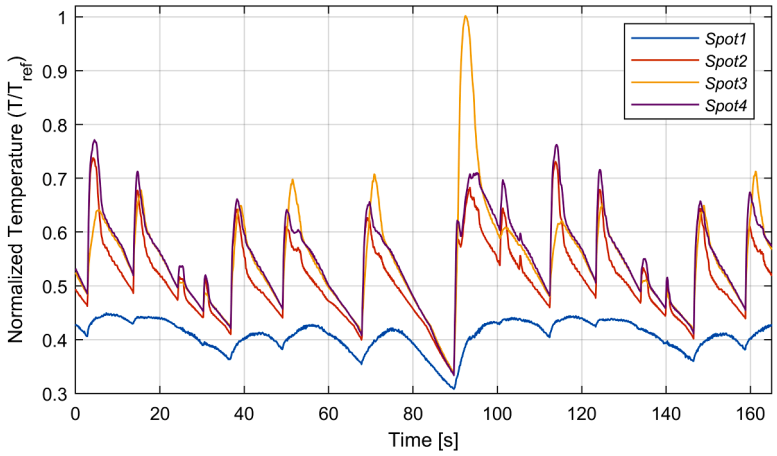


**Fig 2.** Normalized temperatures measured at four radial distances with the multi-spot sensor over about two consecutive laps in the race track used for tests.

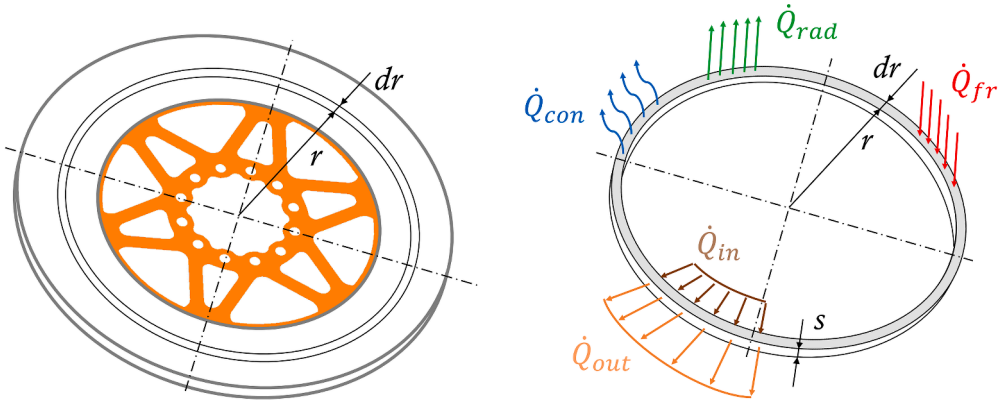


**Fig 3.** Infinitesimal ring of the brake disc.

$$f(r) = \begin{cases} w_i \cdot \dfrac{\dot{Q}_{BRK}}{\pi \cdot (r_4{}^2 - r_1{}^2)} & if\ r_i < r < r_{i+1} \quad i = 1, \cdots, 3. \\ 0 & elsewhere \end{cases} \tag{6}$$

The total braking power, $\dot{Q}_{BRK}$, is computed as the product of the measured wheel angular speed and the braking torque. The latter is estimated from the measured brake fluid pressure, by assuming a constant friction coefficient: this leads to high uncertainty affecting the value of $\dot{Q}_{BRK}$, since the actual instantaneous friction coefficient undergoes high variability during each braking maneuver. $r_1$ is the internal radius of the pad and $r_4 = r_{est}$. The contact region with the pads has been divided into 3 parts, each one corresponding to the circular crown swept by the corresponding temperature sensor available in the disc-pads contact patch, hence:

$$r_{i+1} - r_i = \frac{(r_4 - r_1)}{3} \tag{7}$$

In each circular crown the power distribution is assumed to be constant, and its value is identified through the weighting parameter $w_i$. Any positive value can be selected as long as the following condition ensuring the conservation of the total power is met:

$$\sum_{i=1}^{3} \pi \cdot \left(r_{i+1}{}^2 - r_i{}^2\right) \cdot w_i = \pi \cdot \left(r_4{}^2 - r_1{}^2\right) \tag{8}$$

It is worth noting that only in Section 5.2 the power distribution is modified to improve the UKF temperature prediction, whereas it is considered uniform for all the other applications presented, i.e. $w_1 = w_2 = w_3 = 1$. However, also in the latter case, $\dot{Q}_{fr}$ is still a function of the radius because its contribution is null outside the disc/pads contact region.

By performing the power balance in Eq. (9), it is possible to derive the partial differential equation (PDE) that governs the heat exchange of the reference volume, Eq. (10).

$$\dot{Q}_{in} - \dot{Q}_{out} = \dot{Q}_{con} + \dot{Q}_{rad} - \dot{Q}_{fr} + \frac{\partial U}{\partial t} \tag{9}$$

$$c_v \rho \frac{\partial T}{\partial t} - \frac{1}{r}\frac{\partial}{\partial r}\left(K_c r \frac{\partial T}{\partial r}\right) + \frac{2h}{s}(T - T_{amb}) = g(r,t) \tag{10}$$

where $U$ is the internal energy of the disc, $c_v$ is specific heat, $\rho$ is the density, and $g$ is a generic function taking into account the heat dissipated by radiation and the one generated by friction.

The following equations are known as Robin boundary conditions and define the heat flux at the boundary:

$$K_c \frac{\partial T}{\partial r}(r_{int}, t) = h\ (T(r_{int}, t) - T_{amb}) \tag{11}$$

$$K_c \frac{\partial T}{\partial r}(r_{est}, t) = h\ (T_{amb} - T(r_{est}, t)\ ) \tag{12}$$

where $r_{\mathrm{int}}$ and $r_{\mathrm{est}}$ represent the internal and external radius at which these conditions are applied, $T_{\mathrm{amb}}$ is the ambient temperature, $K_c$ is the thermal conductivity and $h$ is the convection coefficient. For sake of simplicity, only convection is simulated at the extremities of the disc geometry, corresponding to the inner and outer cylindrical surfaces.

Finally, the initial temperature distribution on the disc is:

$$T(r,0) = l(r) \tag{13}$$

The finite element approach reduces the PDE of Eq. (10) into the following ordinary differential equation:

$$\mathbf{M}\cdot\frac{d}{dt}\begin{Bmatrix} T_{node1} \\ \vdots \\ T_{nodeN} \end{Bmatrix} + (\mathbf{A}_{cond} + \mathbf{A}_{conv})\cdot\begin{Bmatrix} T_{node1} \\ \vdots \\ T_{nodeN} \end{Bmatrix} = \mathbf{p} \tag{14}$$

where $\mathbf{M}$ is the heat capacity matrix, $T_{\text{node-i}}$ represents the temperature corresponding to the $i$-th node of the model, $\mathbf{p}$ is the vector that contains the heat generated by friction and radiation, $\mathbf{A}_{\text{cond}}$ is the matrix representing conduction and $\mathbf{A}_{\text{conv}}$ is the one representing convection. Integrating Eq. (14) through time using the Backward Euler method brings about the solution of the temperature field on the disc:

$$\begin{Bmatrix} T_{node1,k} \\ \vdots \\ T_{nodeN,k} \end{Bmatrix} = \left(\left(\frac{\mathbf{M}}{t}\right) + \left(\mathbf{A}_{cond_{k-1}} + \mathbf{A}_{conv_{k-1}}\right)\right) \backslash \left(\left(\frac{\mathbf{M}}{t}\right)\cdot\begin{Bmatrix} T_{node1,k-1} \\ \vdots \\ T_{nodeN,k-1} \end{Bmatrix} + \mathbf{p}_{k-1}\right) \tag{15}$$

where $\Delta t$ is the time step of each iteration. Note that the two matrices $\mathbf{A}_{\text{conv}}$ and $\mathbf{A}_{\text{cond}}$ cannot be defined for the current time step because they contain some parameters that depend on temperature, such as the specific heat and the value of thermal conductivity of the disc. Hence, they are defined using the results of the previous time step. To avoid the introduction of a temperature vector raised to the fourth power, also the energy dissipated by radiation is calculated considering the temperature of the previous time step and inserted in the known vector $\mathbf{p}$. In this way, the continuous temperature gradient along the radius of the disc is simplified as a discrete sequence of concentric ring-shaped regions in which the temperature varies linearly, as shown in Fig. 4.

Different mesh sizes are considered for the 1D-FE model, depending on the task to be accomplished, i.e. either parameter identification or state estimation. As for the first task, i.e. for the convection heat transfer coefficient identification process, a finer mesh of 51 nodes equally spaced along the disc radius is adopted to discretize the brake disc. Indeed, such process is performed only once for each brake configuration, hence higher computational requirements being acceptable. Conversely, a coarser mesh of only 10 nodes is implemented in the 1D-FE model adopted for temperature estimation, in order to significantly reduce the execution time of the algorithm. A justification for the latter choice is provided in Section 5.2.

As for the sampling frequency, the 1D-FE model runs at 10 Hz and its integration through time is solved using the Backward Euler method that ensures numerical stability.

The properties of the material (the specific heat capacity and the thermal conductivity) were provided by the brake disc manufacturer. Therefore, the remaining unknown parameter that is required for the complete definition of the thermal model is the overall convection heat transfer coefficient of the disc, $h$. Since $h$ is quite difficult to calculate (being affected by multiple factors, such as velocity, steering angle and roll angle), it is estimated by the UKF itself (see Section 4.1).

## 4. Unscented Kalman Filter implementation

Kalman filters belong to a category of optimal estimation algorithms (called Bayesian recursive filters) that are used for estimating the state at the $k$-th time step, $\mathbf{x}_k$, of a time-varying system which is indirectly observed through noisy measurements $\mathbf{y}_1$, …, $\mathbf{y}_k$. Consistently with the theory of state observers (e.g. see Sarkka [22]), a dynamic system can be represented by using two sets of equations that the filters operates on, namely the state–transition, Eq. (16), and the observation or measurement model, Eq. (17):

$$\mathbf{x}_k = \mathbf{f}_{k-1}(\mathbf{x}_{k-1}) + \mathbf{q}_{k-1} \tag{16}$$

$$\mathbf{y}_k = \mathbf{g}_k(\mathbf{x}_k) + \mathbf{r}_k \tag{17}$$

where $\mathbf{x}_k \in \mathbb{R}_n$ is the state vector, $\mathbf{y}_k \in \mathbb{R}_m$ is the measurement vector, $\mathbf{q}_{k-1} \sim N(\mathbf{0}, \mathbf{Q}_{k-1})$ is the Gaussian process noise that measures the uncertainty of the physical model prediction ($\mathbf{Q}_{k-1}$ being the corresponding covariance matrix), $\mathbf{r}_k \sim N(\mathbf{0}, \mathbf{R}_k)$ is the Gaussian measurement noise which is related to the sensor accuracy ($\mathbf{R}_k$ being the corresponding covariance matrix), $\mathbf{f}_{k-1}$ is the dynamic model function, and $\mathbf{g}_k$ is the measurement model function. Therefore, the time evolution of the state is represented as a dynamic system which is perturbed by a certain process noise, which is used for modeling the uncertainties in the system dynamics, Eq. (16). Similarly, the introduction of some measurement noise in Eq. (17) prevents the sensor acquisitions from being deterministic functions of the true state of the system.

Bayesian filters recursively estimate the unknown variables of the system combining the series of measurements observed over time with the predictions made by the dynamic model. This process requires computing the marginal posterior distribution$p(\mathbf{x}_k|\mathbf{y}_{1:k})$ of the system state vector at each time step $k$ given the history of the measurements up to the time step $k$. Recalling the Bayesian inference theory,$p(\mathbf{x}_k|\mathbf{y}_{1:k})$ can be rewritten as:

$$p(\mathbf{x}_k|\mathbf{y}_{1:k}) = p(\mathbf{y}_k|\mathbf{x}_k)\cdot p(\mathbf{x}_k|\mathbf{y}_{1:k-1})/z_k \tag{18}$$

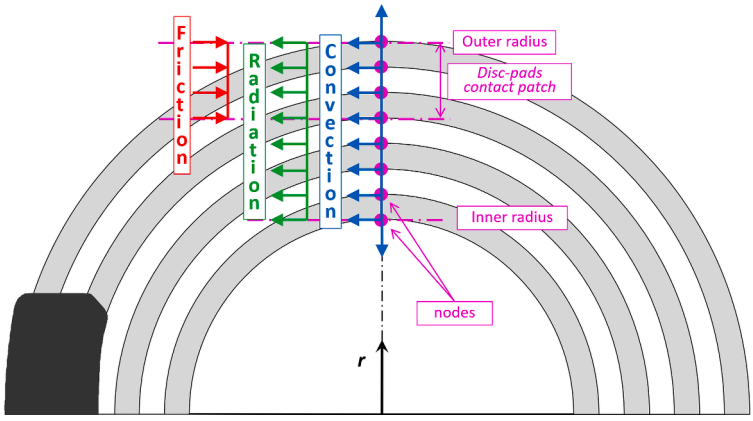


**Fig 4.** Schematic of the 1D-FE model with equally spaced nodes along the disc radius.

where:

$$p(\mathbf{x}_k|\,\mathbf{y}_{1:k-1}) = \\ = \int p(\mathbf{x}_k|\,\mathbf{x}_{k-1})\cdot p(\mathbf{x}_{k-1}|\,\mathbf{y}_{1:k-1})\cdot d\mathbf{x}_{k-1} \tag{19}$$

$$z_k = \int p(\mathbf{y}_k|\,\mathbf{x}_k)\cdot p(\mathbf{x}_k|\,\mathbf{y}_{1:k-1})\cdot d\mathbf{x}_{k-1} \tag{20}$$

Through these recursive equations derived from Bayes' theorem, it is possible to express the posterior distribution of the current state $p(\mathbf{x}_k|\,\mathbf{y}_{1:k})$ starting from the knowledge of the prior probability $p(\mathbf{x}_k|\mathbf{y}_{1:\,k-1})$ and the likelihood function $p(\mathbf{y}_k|\mathbf{x}_k)$. The likelihood coincides directly with the measurement model, while in Eq. (19), the posterior distribution from the previous time step is combined with the prediction performed by the dynamic model$p(\mathbf{x}_k|\mathbf{x}_{k-1})$ to generate the current prior distribution. Therefore, once the dynamic and measurement models are defined, Bayesian inference provides the equations for computing the posterior distributions and point estimates for any problem. The Linear Kalman filter [22] represents the closed form solution to the Bayesian filtering equations when the dynamic and measurement models are linear Gaussian, hence when Eqs. (16) and (17) can be rewritten in probabilistic terms as:

$$\begin{aligned} p(\mathbf{x}_k|\,\mathbf{x}_{k-1}) &= N(\mathbf{x}_k\,|\,\mathbf{f}_{k-1}(\mathbf{x}_{k-1}),\mathbf{Q}_{k-1}) = \\ &= N(\mathbf{x}_k\,|\,\mathbf{A}_{k-1}\cdot\mathbf{x}_{k-1},\mathbf{Q}_{k-1}) \end{aligned} \tag{21}$$

$$\begin{aligned} p(\mathbf{y}_k|\,\mathbf{x}_k) &= N(\mathbf{y}_k\,|\,\mathbf{g}_k(\mathbf{x}_k),\mathbf{R}_k) = \\ &= N(\mathbf{y}_k\,|\,\mathbf{H}_k\cdot\mathbf{x}_k,\mathbf{R}_k) \end{aligned} \tag{22}$$

where $\mathbf{A}_{k-1}$ and $\mathbf{H}_k$ are the matrices describing the linearization of functions $\mathbf{f}_{k-1}$ and $\mathbf{g}_k$, respectively. Under these assumptions, the Bayesian filtering Eqs. (18–20) for the linear filtering model of Eqs. (21, 22) can be evaluated in closed form. The resulting distributions are Gaussian

$$p(\mathbf{x}_k|\,\mathbf{y}_{1:k-1}) = N\left(\mathbf{x}_k\,|\,\mathbf{m}_k^-,\,\mathbf{P}_k^-\right) \tag{23}$$

$$p(\mathbf{y}_k|\,\mathbf{y}_{1:k-1}) = N\left(\mathbf{y}_k\,|\,\mathbf{H}_k\cdot\mathbf{m}_k^-,\,\mathbf{P}_k^-\right) \tag{24}$$

$$p(\mathbf{x}_k|\,\mathbf{y}_{1:k}) = N((\mathbf{x}_k|\,\mathbf{m}_k,\mathbf{P}_k) \tag{25}$$

where the superscript "-" indicates the prior estimation, and the mean $\mathbf{m}_k$ and the covariance $\mathbf{P}_k$ of the posterior distribution$p(\mathbf{x}_k|\mathbf{y}_{1:k})$ can be determined by recursively computing the following Kalman filter prediction and update steps:

Prediction

$$\mathbf{m}_k^- = \mathbf{A}_{k-1}\cdot\mathbf{m}_{k-1} \tag{26}$$

$$\mathbf{P}_k^- = \mathbf{A}_{k-1}\cdot\mathbf{P}_{k-1}\cdot\mathbf{A}_{k-1}^T + \mathbf{Q}_{k-1} \tag{27}$$

Updating

$$\mathbf{S}_k = \mathbf{H}_k\cdot\mathbf{P}_k^-\cdot\mathbf{H}_k^T + \mathbf{R}_k \tag{28}$$

$$\mathbf{K}_k = \mathbf{P}_k^-\cdot\mathbf{H}_k^T\cdot\mathbf{S}_k^{-1} \tag{29}$$

$$\mathbf{m}_k = \mathbf{m}_k^- + \mathbf{K}_k\cdot\left(\mathbf{y}_k - \mathbf{H}_k\cdot\mathbf{m}_k^-\right) \tag{30}$$

$$\mathbf{P}_k = \mathbf{P}_k^- - \mathbf{K}_k\cdot\mathbf{S}_k\cdot\mathbf{K}_k^T \tag{31}$$

In case the dynamic model is not linear, the Linear Kalman filter is not appropriate and must be replaced either by the Extended Kalman filter (EKF) or the Unscented Kalman filter (UKF). Both the EKF and the UKF approximate the filtering distributions as Gaussian so that Eqs. (16, 17) can be rewritten as Eqs. (21, 22). The EKF approximates the nonlinear and non-Gaussian models by linearizing the functions $\mathbf{f}_{k-1}(\mathbf{x}_{k-1})$ with a Taylor series expansion. Conversely, the UKF uses the *unscented transform* to directly approximate the mean and covariance of the target distribution. Instead of linearizing $\mathbf{f}_{k-1}(\mathbf{x}_{k-1})$ in Eq. (16) to ensure that$p(\mathbf{x}_k|\mathbf{x}_{k-1})$ in Eq. (21) is linear Gaussian, the UKF draws some elements from the prior distribution (called sigma points) and passes them directly through the nonlinear function $\mathbf{f}_{k-1}(\mathbf{x}_{k-1})$, obtaining another set of points (called transformed sigma points). Each sigma point constitutes a state vector of the system: once they are transformed through the nonlinear function, they belong to a new arbitrary distribution. The unscented transform computes the Gaussian that better fits the transformed sigma points, approximating the nonlinearly transformed mean and covariance. Finally, these parameters are used to calculate the new state estimate as in Eq. (21). Given the filtering distributions shown in (Eqs. 23–25), the operations performed by the UKF at each measurement step to finally calculate $\mathbf{m}_k$ and $\mathbf{P}_k$ are the following:

Prediction

- Form the sigma points: given a $n$-order state vector, $2n + 1$ sigma points are selected around its mean value $\mathbf{m}_{k-1}$,

$$\chi_{k-1}^{(0)} = \mathbf{m}_{k-1} \tag{32}$$

$$\chi_{k-1}^{(i)} = \mathbf{m}_{k-1} + \sqrt{n+\lambda}\cdot\left[\sqrt{\mathbf{P}_{k-1}}\right]_i \tag{33}$$

$$\chi_{k-1}^{(i+n)} = \mathbf{m}_{k-1} - \sqrt{n+\lambda}\cdot\left[\sqrt{\mathbf{P}_{k-1}}\right]_i,\ i = 1,\ \cdots,\ n \tag{34}$$

where $\lambda$ is a filter parameter.

- Propagate the sigma points through the dynamic model:

$$\widehat{\chi}_k^{(i)} = \mathbf{f}_{k-1}\left(\chi_{k-1}^{(i)}\right),\ i = 1,\cdots,\ 2n \tag{35}$$

- Intermediate estimates for the propagated state and covariance matrix (predicted mean $\mathbf{m}_k^-$ and the predicted covariance $\mathbf{P}_k^-$) are computed by weighted averages:

$$\mathbf{m}_k^- = \sum_{i=0}^{2n} W_i^{(m)}\widehat{\chi}_k^{(i)} \tag{36}$$

$$\mathbf{P}_k^- = \sum_{i=0}^{2n} W_i^{(c)}\cdot\left(\widehat{\chi}_k^{(i)} - \mathbf{m}_k^-\right)\cdot\left(\widehat{\chi}_k^{(i)} - \mathbf{m}_k^-\right)^T + \mathbf{Q}_{k-1} \tag{37}$$

where the weights are calculated as: $W_i^{(c)} = W_i^{(m)} = 1/[2(n+\lambda)],\ i = 1,\ldots,2n$ and $W_0^{(m)} = W_0^{(c)} = \lambda/(n+\lambda)$ .

Updating

- Form the sigma points:

$$\chi_k^{-(0)} = \mathbf{m}_k^- \tag{38}$$

$$\chi_k^{-(i)} = \mathbf{m}_k^- + \sqrt{n+\lambda}\cdot\left[\sqrt{\mathbf{P}_k^-}\right]_i \tag{39}$$

$$\chi_k^{-(i+n)} = \mathbf{m}_k^- - \sqrt{n+\lambda}\cdot\left[\sqrt{\mathbf{P}_k^-}\right]_i,\ i = 1,\ \cdots,\ n \tag{40}$$

- Propagate sigma points through the measurement model:

$$\widehat{\mathbf{Y}}_k^{(i)} = \mathbf{g}_k\left(\chi_k^{-(i)}\right),\ i = 0,\cdots,2n \tag{41}$$

- Compute the predicted mean $\boldsymbol{\mu}_k$, the predicted covariance of the measurement $\mathbf{S}_k$, and the cross-covariance of the state and the measurement $\mathbf{C}_k$:

$$\boldsymbol{\mu}_k = \sum_{i=0}^{2n} W_i^{(m)} \cdot \widehat{\mathbf{Y}}_k^{(i)} \tag{42}$$

$$\mathbf{S}_k = \sum_{i=0}^{2n} W_i^{(c)} \cdot \left(\widehat{\mathbf{Y}}_k^{(i)} - \boldsymbol{\mu}_k\right) \cdot \left(\widehat{\mathbf{Y}}_k^{(i)} - \boldsymbol{\mu}_k\right)^T + \mathbf{R}_k \tag{43}$$

$$\mathbf{C}_k = \sum_{i=0}^{2n} W_i^{(c)} \cdot \left(\widehat{\boldsymbol{\chi}}_k^{-(i)} - \mathbf{m}_k^-\right) \cdot \left(\widehat{\mathbf{Y}}_k^{(i)} - \boldsymbol{\mu}_k\right)^T \tag{44}$$

- Finally compute the filter gain$\mathbf{K}_k$, the filtered state mean $\mathbf{m}_k$, and the covariance $\mathbf{P}_k$, conditional on the measurement $\mathbf{y}_k$

$$\mathbf{K}_k = \mathbf{C}_k \cdot \mathbf{S}_k^{-1} \tag{45}$$

$$\mathbf{m}_k = \mathbf{m}_k^- + \mathbf{K}_k \cdot (\mathbf{y}_k - \boldsymbol{\mu}_k) \tag{46}$$

$$\mathbf{P}_k = \mathbf{P}_k^- - \mathbf{K}_k \cdot \mathbf{S}_k \cdot \mathbf{K}_k^T \tag{47}$$

The above UKF derivation is common to all implementations of state and parameter estimation, so the simple substitution of $\mathbf{x}$ in the above with the actual state vector, used in the applications reported in Sections 4.1 and 4.2, provides the identifying filter.

The UKF is based on the idea that approximating a nonlinear statistical distribution is easier and more accurate than linearizing a nonlinear function, as the EKF does. Indeed, the UKF ensures accurate results and, unlike the EKF, it does not require computing the model Jacobians, hence being more efficient and easier to implement. Another advantage is that the UKF is not based on a linear approximation at a single point, but uses further points in approximating the nonlinearity. Given the advantages of the UKF with respect to the EKF in case of a nonlinear system, the former algorithm has been implemented in this study. Even though the UKF manages the nonlinearity of the model and it is relatively easy to implement, it can be computationally very expensive due to the unscented transform involved in the algorithm. As pointed out by Bogdanski et al. [20], as the number of parameters increases, the UKF has more sigma points to process at each time step. Therefore, it does not appear suitable for FE models with higher dimensions for the problem of interests. In the application proposed in this article, the UKF is used for computing the actual temperature distribution on the disc radius, so that both the measurements and the assumed dynamics (FE model of the brake) are taken into account. The UKF is also successfully employed to identify the convection coefficient of the brake, $h$: as discussed in Section 4.1, $h$ can be estimated simultaneously with the true states of the system by concatenating $h$ to the state vector and adapting the filter architecture.

The flowchart shown in Fig. 5 summarizes the use of the UKF in the two consecutive phases of the proposed method (i.e., firstly as a parameter identifier for $h$ and then as a state observer for the disc temperature), described in Sections 4.1 and 4.2. The UKF has been implemented by making the following assumptions:

- the dynamic model of the disc temperature is given by the 1D-FE model and Gaussian noise;
- the variation model for $h$ is unknown (Gaussian random walk);

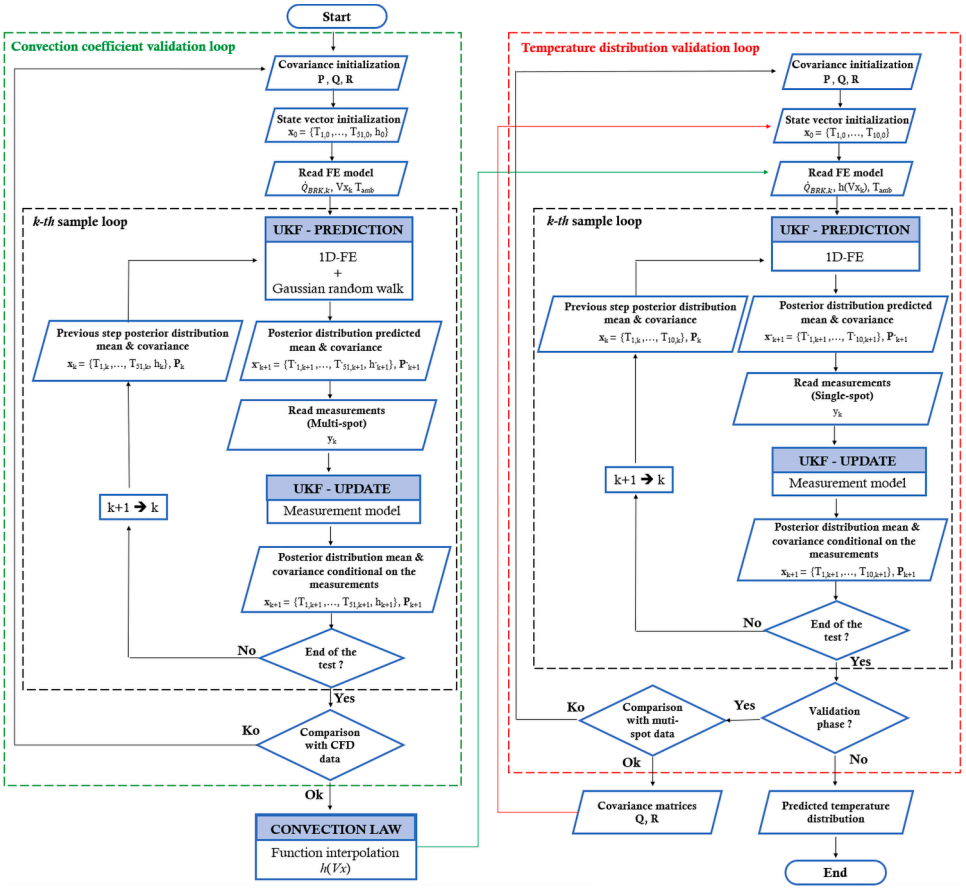


**Fig 5.** Flowchart describing the UKF implementation for the proposed method.

- the measuring model is a linear interpolation of the state vector and Gaussian noise.

### 4.1. Convection heat transfer coefficient identification

When the UKF filter is used as a parameter identifier, in addition to the temperature values of the nodes, the state vector contains also the convection coefficient to be identified. In this scenario the dynamic model does not coincide with the 1D-FE model of Eq. (15) and $\mathbf{f}_{k-1}(\mathbf{x}_{k-1})$ is not linear with respect to the augmented state vector. The temperature of the nodes depends on the convection coefficient through the matrix $\mathbf{A}_{conv,k-1}$. By making this dependency explicit, the dynamic model is no longer linear with respect to the state vector and the linear Kalman filter cannot be used. Therefore, the dynamic model Eq. (13) becomes:

$$\begin{Bmatrix} \mathbf{x}_k \\ h_k \end{Bmatrix} = \begin{Bmatrix} \mathbf{f}_{k-1}(\mathbf{x}_{k-1},\ h_{k-1}) \\ h_{k-1} \end{Bmatrix} + \begin{Bmatrix} \mathbf{q}_{k-1} \\ \varepsilon_{k-1} \end{Bmatrix} \tag{48}$$

where $\mathbf{f}_{k-1}$ corresponds to the 1D-FE model of Eq. (15), $\varepsilon_{k-1} \sim N(0, e_{k-1})$ and

$$\mathbf{x}_k = \begin{pmatrix} T_{node1,k} \\ \vdots \\ T_{nodeN,k} \end{pmatrix} \tag{49}$$

Essentially, since it is not clear how $h$ can be calculated through a proper physical model, Eq. (48) allows $h$ to perform a Gaussian random walk between time steps. The dynamic model equation can be brought back to a more convenient formulation by including $h$ in the state vector $\mathbf{x'}_k$.

$$\mathbf{x}'_k = \begin{pmatrix} T_{node1,k} \\ \vdots \\ T_{nodeN,k} \\ h_k \end{pmatrix} = \mathbf{z}_{k-1}\left(\mathbf{x}'_{k-1}\right) + \mathbf{q}'_{k-1} \tag{50}$$

where

$$\mathbf{z}_{k-1} = \begin{Bmatrix} \mathbf{f}_{k-1}\left(\mathbf{x}'_{k-1}\right) \\ h_{k-1} \end{Bmatrix} \tag{51}$$

$$\mathbf{q}'_{k-1} = \begin{Bmatrix} \mathbf{q}_{k-1} \\ \varepsilon_{k-1} \end{Bmatrix} \tag{52}$$

To ensure an accurate estimate, all the four measurements available were used for the identification of the convection coefficient. The measurement model is therefore represented by the linear interpolation of the node temperatures in the center of the four sensor measurement surfaces:

$$\mathbf{y}_k = \begin{pmatrix} T_{spot1,k} \\ T_{spot2,k} \\ T_{spot3,k} \\ T_{spot4,k} \end{pmatrix} = \mathbf{H}_k \cdot \mathbf{x}_k + \mathbf{r}_k \tag{53}$$

where and the matrix $\mathbf{H}_k$ performs the linear interpolation of the temperatures corresponding to the two nodes closest to the spots at which the measurement is taken. The UKF architecture described by Eqs. (50, 53) is based on highly reliable temperature measurements, and an accurate thermal model of the disc whose precision is partially hindered by the weak mathematical model for $h$. Through a trial–and–error procedure, acting on the covariance matrices of the process and measurement errors (i.e. on $\mathbf{R}_k$, $\mathbf{Q}_{k-1}$ and $e_{k-1}$) it is possible to calibrate the model so that every time there is a relevant difference between the measured and predicted temperature values, the filter will trust the information coming from the sensors and will update the prediction performed by the model. Since $h$ is the most unreliable state variable, the filter predominantly adjusts its value of a quantity proportional to the error generated, so that the temperature difference is reduced. By solving this optimization problem, the filter is able to find the parameter value that allows the temperature estimated through the thermal model to get as close as possible to the measured ones. Since the model is a good approximation of the reality, as soon as the measured temperatures match the estimated ones the model is likely to converge to the real system. Therefore, it can be stated that the parameter that the filter estimates is likely to converge to the real one [23]. Once $h$ is identified, a law for the variation of $h$ with respect to the forward velocity of the vehicle is implemented in the 1D-FE model by interpolating the cloud of values estimated with the UKF (see Fig. 6 in Section 5). This interpolation was performed considering only the samples in off-brake condition (i.e. in the cooking phase out of the braking maneuver). In fact, the differences in the way energy enters the system between the mathematical model (uniformly with the radius) and the reality (which seems to be more affected by the pressure distribution in the caliper and the pads wear state, as shown in Section 2) lead the UKF to output some unreliable values for $h$ during braking.

### 4.2. Temperature estimation

Once the convection coefficient has been identified, the 1D-FE model could be used directly to perform the disc temperature estimation. However, to account for external factors that are not simulated in the FE model, it was deemed convenient to still rely on the UKF for more accurate predictions. Therefore, the UKF architecture is adapted to predict the temperature of the nodes. In particular, being the state vector $\mathbf{x}_k$ composed of node temperatures only, this time the dynamic system of the filter coincides with the 1D-FE model. It's important to remark that the measurement model must be adapted as well. Indeed, during the race, only the measurement of the single-spot sensor is available. Hence, $y_k$ is no longer a vector. Eqs. (50, 53) become:

$$\mathbf{x}_k = \begin{pmatrix} T_{node1,k} \\ \vdots \\ T_{nodeN,k} \end{pmatrix} = \mathbf{f}_{k-1}(\mathbf{x}_{k-1}) + \mathbf{q}_{k-1} \tag{54}$$

$$y_k = \mathbf{H}_k \cdot \mathbf{x}_k + r_k \tag{55}$$

where, $\mathbf{f}_{k-1}(\mathbf{x}_{k-1})$ is equal to Eq. (15), $\mathbf{q}_{k-1} \sim N(\mathbf{0}, \mathbf{Q}_{k-1})$ is the Gaussian process noise,$y_k = T_{spot3,k}$, $r_k \sim N(0, R_k)$ is the Gaussian measurement noise and $\mathbf{H}_k$ is the measurement model matrix. The latter performs the linear interpolation of the temperatures corresponding to the two nodes closest to the center of the measurement surface of *Spot3*.

Although the filter architecture is changed, the operations performed by the UKF at each time step are the same as the one described previously by Eqs. (32–47).

## 5. Results and discussion

### 5.1. Assessment of the convection heat transfer coefficient identification

In absence of power generated by friction (i.e. during the braking maneuver) the model is expected to provide a good approximation of the reality, hence the estimated values being quite accurate. To assess the reliability of the value of $h$, a comparison with the results obtained through CFD simulation is made. In order to keep the simulation as simple and fast as possible, it was performed considering only the

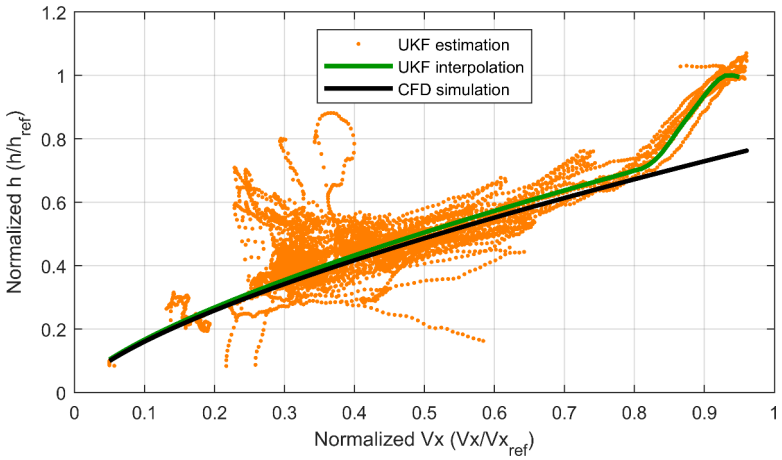


**Fig 6.** Normalized convection coefficient as a function of the normalized forward speed.

influence of the forward velocity, *Vx*, whereas the effects of both the steering angle and the roll angle were disregarded. The calculation was carried out only at three specific speed values and then the black curve shown in Fig. 6 was extrapolated for all the other velocity values. Even though the CFD analysis is oversimplified, the result obtained through this comparison is crucial to assess the reliability of the estimated convection coefficient and its relevance to reality.

Fig 6 reports the estimated values of $h$ as a function of the forward speed. Both quantities are normalized with respect to reference values (namely, $h_{ref}$ and $Vx_{ref}$, respectively). The low-speed region of the graph results quite noisy. This behavior should be ascribable to the uncertainty related to the temperature distribution passed to the UKF as initial condition at the beginning of the estimation. Conversely, the estimated values of $h$ appear highly coherent in the mid/high-speed region. The UKF estimates have been interpolated to obtain a curve (solid green line) that can be directly compared with the CFD results. In particular, as a modification in the trend of the estimated values can be clearly observed at a normalized speed $Vx$ of about 0.8, two distinct interpolating curves (functions of $Vx$) have been exploited. For $Vx < 0.8$, a power function has been adopted; for $Vx \geq 0.8$, a cubic polynomial has been used; the two functions are joined at $Vx = 0.8$ to achieve a continuous curve. The interpolated $h$ curve closely matches the trend of the CFD simulations in most of the velocity domain, hence confirming the robustness off the proposed parameter identification approach. Discrepancies can be observed above a normalized speed of about 0.8, where the values of $h$ increase considerably and apparently diverge from the CFD results. The source of this phenomenon is still under investigation. Deeper investigations are being performed through additional CFD simulations, by modelling the deformations of the tire cross section as a function of the wheel angular velocity (whereas tire deformations had been neglected in the first simulations). Indeed, the preliminary results provided by such analyses showed that the tire deformations beyond a normalized $Vx$ of 0.8 might completely expose the disc to the undisturbed air flow, thus ensuring a faster cooling of the disc. Hence, these results seem to confirm the correctness of the UKF identification approach, which was therefore capable of revealing an unexpected behavior that went initially unnoticed by the CFD simulation standardly adopted by the company for the analysis.

In the end, the interpolated values of $h$ are implemented in the 1D-FE model for a more accurate temperature estimation.

### 5.2. Analysis of the 1D-FE temperature estimation performance

The results obtained with different mesh sizes of the 1D-FE model have been investigated in order to determine the optimal number of nodes for the final algorithm. The analysis has been performed by starting from 150 nodes and reducing the mesh size till a minimum 10 nodes (which is the limit value to have at least 1 node for each spot of the temperature transducer). The results of the analysis for the temperature of *Spot3* are reported in Table 2 for the most relevant mesh sizes. The variation in the estimation of the temperature distribution has been evaluated in terms of the Root Mean Squared Error (RMSE) with respect to the 150-noded model, over the reference lap. The table also show the computational time required for processing the samples of one lap, for the 1D-FE alone and for the complete algorithm including the UKF.

It can be observed that the temperatures predicted by the 10-noded model do not differ remarkably from those obtained with a finer mesh, in terms of RMSE. Conversely, the increment in the computational time appears not negligible. In particular, the UKF can become computationally very expensive due to the unscented transform. Indeed, as the number of parameters increases, the UKF has more sigma points to process at each time step. Since every iteration of the UKF requires running the 1D-FE model, the resulting algorithm is extremely slow.

In addition, the trend of the predicted temperature over the reference lap is shown in Fig. 7 for some of the tested mesh sizes. It can be observed that, despite using more nodes, the temperature peak of *Spot3* remains not accurately reconstructed. Actually, the introduction of a finer mesh may even worsen the peak prediction in some cases (due to a combined effect of how the nodes approximate each region and how he braking power has been defined)

In light of the above considerations, a 10-noded mesh has been selected as the optimal mesh size for the final temperature estimation algorithm.

### 5.3. Accuracy of the UKF temperature estimate

Once the convection heat transfer coefficient has been identified, the temperature estimation is performed using only the measurement of *Spot3*. The acquisitions made in the other measurement spots are used for validation purpose only.

In Fig. 8 the temperature measured experimentally (black solid line,

**Table 2**
Performance of the FE model for different mesh sizes.

| Nodes | RMSE (Normalized *T Spot3*) | 1D-FE computational time [s/lap] | UKF computational time [s/lap] |
|---|---|---|---|
| 150 | - | 1.24 | 373.24 |
| 100 | 0.0002 | 0.84 | 168.84 |
| 50 | 0.0009 | 0.61 | 61.95 |
| 20 | 0.0015 | 0.41 | 16.95 |
| 10 | 0.0062 | 0.33 | 7.00 |

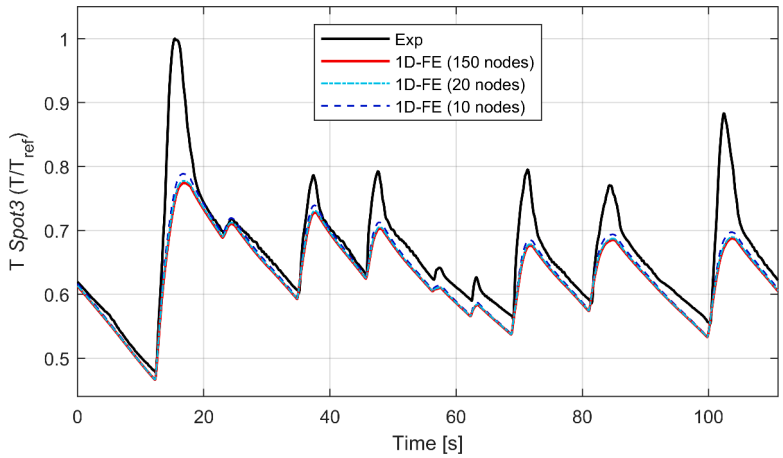


**Fig 7.** Measured (Exp) vs. estimated (1D-FE) normalized temperatures.

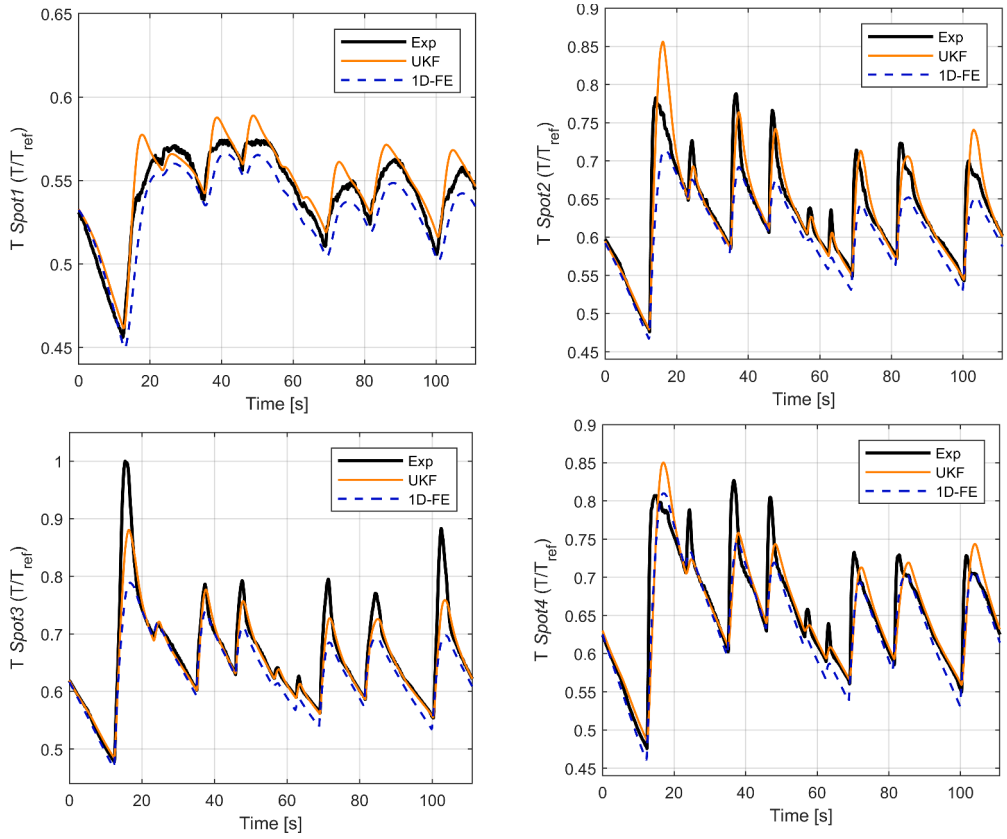


**Fig 8.** Measured (Exp) vs. estimated (UKF & 1D-FE) normalized temperatures.

Exp), the prediction made by the 1D-FE model alone (dashed blue line) and the UKF estimation (solid orange line) are compared over one reference lap of the race track tests.

As expected, the 1D-FE model alone appears unable to predict the large temperature gradient along the disc radius that may be generated during a vigorous braking. This behavior is partially ascribable to the uncertainty affecting both the total braking power entering the system in the braking phase ($\dot{Q}_{BRK}$) and the actual power distribution over the contact patch, $f(r)$. As for the latter aspect, the possibility of implementing a non-uniform pressure distribution to improve the model prediction is currently under investigation. However, as it can be seen in Fig. 2, it appears very difficult to identify a regular pattern in the power distribution related to the measurement area of each spot. Another important consideration is that concentrating the disc mass on one single layer of nodes may increase excessively the thermal inertia of the system and prevents the 1D-FE model from detecting the temperature peaks measured during braking maneuvers. As a result, the 1D-FE model underestimates the maximum temperature registered in the third spot by 22 %. The significant peak underestimation also leads to a general underestimation of the temperature over the entire reference lap. As assessing the temperature of the disc is an essential requirement for accurately estimating the friction coefficient of the brake and its overall performance, such error is deemed not acceptable. Nonetheless, the temperature signals are predicted with high accuracy during the off-brake phases, hence indicating that the convection coefficient identification was successful.

With the introduction of the UKF, the temperature prediction is significantly improved. For instance, the discrepancy on the maximum temperature of the disc (related to *Spot3*) is reduced to about 12 %. To compensate for the approximation introduced by the simplified 1D-FE model that lead to the underestimation of the temperature peaks, the weighting parameters, $w_i$, of the power density function $f(r)$ in Eq. (6) were adjusted to move part of the braking power from *Spot3* to *Spot2*. In particular, the new distribution provides 45 % of the total braking power to the nodes related to *Spot2* and 20 % to those related to *Spot3*. By concentrating more power in *Spot2*, the temperature peaks in this region are more accurately reproduced by the FE model at the expense of *Spot3*. However, the accuracy for *Spot3* is ensured by the presence of the single-spot measurement used by the UKF to correct the unbalanced prediction of the FE model, thus obtaining an improvement in the temperature prediction in most of the disc-pad contact patch. The algorithm appears to satisfactorily compensate for the approximations introduced by the simplified 1D-FE model. It can be noticed that some of the temperature peaks related to the fast transients occurring during the braking maneuvers are not properly reconstructed. In particular, a higher underestimation of the peak temperature of *Spot3* is generally associated with an overestimation of the peaks related to the other spots. This effect, clearly observable for the first and the last braking maneuvers of the reference lap shown in Fig. 8, is caused by the UKF gain being determined from the predicted and the measured *Spot3* temperatures. Additional test with different power distributions are still being performed to possibly improve the prediction, particularly for *Spot4*.

The performance of the proposed UKF-based estimation method has been assessed by using the RMSE. The RMSE values (computed with respect to the experimental data provided by the multi-spot sensor) for the UKF and the 1D-FE estimated temperatures reported in Fig. 8 are shown in Table 3. The table also reports the RMSE that would be achieved by assuming the temperatures of *Spot2* and *Spot4* equal to the measurement provided by the single-spot sensor (*Spot3*), i.e. the approach actually adopted in the past. The UKF reduces considerably the error that would be obtained with the 1D-FE model alone, for *Spot1-3*. In particular, for *Spot2* and *Spot3* the error is reduced of about 27 % and 37 %, respectively. Conversely, the performance slightly worsens for *Spot4*. This is reasonably ascribable to the fact that, although the temperature peaks are better predicted by the UKF, the estimated curve exhibits some kind of delay with respect to the measured signal. The UKF also significantly improves the results for both *Spot2* and *Spot4* in comparison with the use of the single-spot sensor. In particular, the error is reduced by almost 50 % for *Spot2*. Furthermore, the UKF can provide reliable information on the thermal behavior of the inner region of the disc, whereas no meaningful results can be obtained from the single-spot sensor: such information may be useful to develop a more comprehensive thermal model of the front wheel assembly, including the tire.

In order to better appreciate the improvement provided by the proposed UKF-based approach, the instantaneous average temperature of the disc/pads contact region can be evaluated. In practice, the simple average of the three spots in the disc region of interest (i.e. *Spot2-4*) is computed. Such quantity is essential in order to properly estimate the actual friction coefficient and, in the end, the braking performance. The average temperature computed for the reference lap, i.e. by considering the curves of *Spot2-4* shown in Fig. 8, is reported in Fig. 9. In case of simply relying on the single-spot sensor, the only measurement would be assumed to be representative of the whole disc/pads contact patch. Therefore, the corresponding curve shown is Fig. 9 (grey dotted line) coincides with the *Spot3* measured temperature. The comparison clearly shows that the UKF estimate closely match the real average temperature (black solid line, Exp). Conversely, the single-spot measurement tends to significantly overestimate the real average temperature.

**Table 3**
RMSE values of the curves related to the reference lap.

| | *Spot1* | *Spot2* | *Spot3* | *Spot4* |
|---|---|---|---|---|
| **UKF** | 0.0095 | 0.0260 | 0.0301 | 0.0349 |
| **1D-FE** | 0.0123 | 0.0355 | 0.0478 | 0.0311 |
| **Single-spot** | - | 0.0513 | 0.0 | 0.0385 |

The corresponding RMSE values (computed with respect to the real average temperature) are reported in Table 4. The percentage variation of the RMSE with respect to the RMSE value single-spot approach is also reported. The comparison proves that the UKF approach significantly improves the accuracy of the average temperature estimate. Indeed, the reduction in the RMSE is of more than 17 %, which is deemed as a huge improvement for a racing application. The 1D-FE model alone is confirmed not sufficiently accurate.

Finally, the UKF approach meets the desired computational requirements. The developed algorithm for temperature estimation can process one lap in about 7.5 s (see Table 2).

## 6. Conclusions

This research activity focused on the development of a fast and computationally efficient tool for estimating the temperature distribution of the carbon discs mounted on the racing motorcycles competing in the MotoGP world championship, a topic not yet investigated.

A novel method exploiting an Unscented Kalman Filter for both parameter identification and state estimation has been implemented. The proposed solution combines the UKF with a simple 1D-FE model of the brake, whose convection heat transfer coefficient was completely identified by the filter itself.

The performance of the developed approach has been assessed by using experimental data acquired from a motorcycle performing test sessions in a real race track. The analysis proved that combining, through the UKF, the theoretical prediction performed by the 1D-FE model with the empirical information measured by the sensor available on board makes the algorithm capable of adapting to the external factors that might shift the temperature prediction from the actual temperature of the disc, thus ensuring a satisfactory trade-off between accuracy and execution time. In particular, the following results could be achieved.

- The convection heat transfer coefficient, *h*, could be successfully identified with a satisfactory precision, as confirmed by numerical results from CFD simulations. This permitted to interpolate a curve describing *h* as a function of the forward velocity *Vx*, to tune and enhance the 1D-FE model.
- The temperature distribution of the disc surface could be estimated with an acceptable accuracy, with an improvement of nearly 50 % in the RMSE for *Spot2* and about 10 % for *Spot4*. While the overall trend of the temperature for each disc region is deemed satisfactory, some of the temperature peaks appear not properly reconstructed, the highest error being associated to the *Spot3* (maximum temperature underestimated by about 12 %).
- The implemented tool allowed to better predict the instantaneous average temperature of the disc in the disc/pads contact region, which is closely related to the actual friction coefficient provided by the disc. A reduction of about 17 % in the RMSE of the average temperature UKF estimate (with respect to the single-spot measurements) could be obtained.
- The computational time of the final algorithm meets the desired specifications, with less than 7.5 s being required to process the samples related to a full lap.

Therefore, the developed UKF-based algorithm represents a significant improvement with respect to the current approach, which simply relies on the temperature measurement available from the onboard sensor.

The proposed approach has been included in the data analysis package that is routinely used to process telemetry data by the company

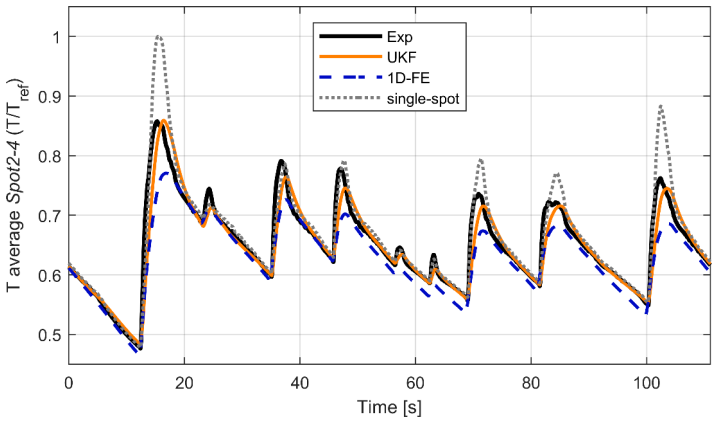


**Fig 9.** Average temperature in the disc/pads contact patch.

**Table 4**
RMSE values for the average temperature.

| | *T average* | *Δ%* |
|---|---|---|
| **UKF** | 0.0236 | −17.3 |
| **1D-FE** | 0.0342 | 19.6 |
| **Single-spot** | 0.0286 | - |

collaborating to the research. The presented solution is deemed essential to estimate the actual braking torque, which heavily depends on the actual temperature distribution of the discs. Furthermore, it will represent a key tool to assess the tire behavior, which is also affected by the thermal dynamics of the braking system.

An improvement of the thermal model is currently under investigation to better estimate the high temperature peaks occurring in the fast thermal transients associated with the hardest braking maneuvers. The possibility of rapidly adapting the FE model for assessing the performance of different aerodynamic configuration of the brake, such as the introduction of a cover for the disc or the usage of ventilated discs, will be also investigated.

## CRediT authorship contribution statement

**Federico Bonini:** Conceptualization, Formal analysis, Investigation, Methodology, Software, Validation, Visualization, Writing – original draft. **Alessandro Rivola:** Funding acquisition, Supervision, Writing – review & editing. **Alberto Martini:** Conceptualization, Formal analysis, Funding acquisition, Project administration, Supervision, Visualization, Writing – original draft, Writing – review & editing.

## Declaration of Competing Interest

The authors declare that they have no known competing financial interests or personal relationships that could have appeared to influence the work reported in this paper.

## Data availability

The data that has been used is confidential.

## Acknowledgments

Ducati Corse is kindly acknowledged for providing real data to test the developed methods. The Authors wish to thank particularly Dr. Nicolò Mancinelli for active collaboration and support.

## References

[1] N. Kumar, A. Bharti, H.S. Goyal, K.K. Patel, The evolution of brake friction materials: a review, Mater. Phys. Mech. 47 (5) (2021) 796–815, https://doi.org/10.18149/MPM.4752021_13.
[2] N.J. Lee, C.G. Kang, The effect of a variable disc pad friction coefficient for the mechanical brake system of a railway vehicle, PLoS ONE 10 (8) (2015), https://doi.org/10.1371/journal.pone.0135459.
[3] T. Hutton, The friction and wear of carbon-carbon composites for aircraft brakes, University of Bath, UK, 1996. PhD thesis.
[4] K. Lee, Numerical Prediction of Brake Fluid Temperature Rise during Braking and Heat Soaking, SAE Technical Paper, 1999, https://doi.org/10.4271/1999-01-0483.
[5] D. Antanaitis, P. Monsere, M. Riefe, Brake system and subsystem design considerations for race track and high energy usage based on fade limits, SAE Int. J. Passenger Cars Mech. Syst. 1 (1) (2009) 689–708, https://doi.org/10.4271/2008-01-0817.
[6] O. Cividini, R. Passoni, Brake Systems and Composite Rotors: How Racing can be a Vision for High Performance Cars, SAE Technical Paper, 2022, https://doi.org/10.4271/2022-01-1174.
[7] A.A. Yevtushenko, M. Kuciej, O. Yevtushenko, Modelling of the frictional heating in brake system with thermal resistance on a contact surface and convective cooling on a free surface of a pad, Int. J. Heat Mass Transf. 81 (2015) 915–923, https://doi.org/10.1016/j.ijheatmasstransfer.2014.11.014.
[8] D. Sheridan, J. Kutchey, F. Samie, Approaches to the thermal modeling of disc brakes, SAE Int. J. Passenger Cars 97 (4) (1988) 268–283, https://doi.org/10.4271/880256.
[9] A. Yevtushenko, M. Kuciej, E. Och, O. Yevtushenko, Effect of the thermal sensitivity in modeling of the frictional heating during braking, Adv. Mech. Eng. 8 (12) (2016), https://doi.org/10.1177/1687814016681744.
[10] F. Talati, S. Jalalifar, Investigation of heat transfer phenomena in a ventilated disk brake rotor with straight radial rounded vanes, J. Appl. Sci. 8 (20) (2008) 3583–3592, https://doi.org/10.3923/jas.2008.3583.3592.
[11] P. Grzes, Finite element analysis of disc temperature during braking process, Acta mechanica et automatica 3 (4) (2009) 36–42.
[12] A.D. McPhee, D.A. Johnson, Experimental heat transfer and flow analysis of a vented brake rotor, Int. J. Therm. Sci. 47 (4) (2007) 458–467, https://doi.org/10.1016/j.ijthermalsci.2007.03.006.
[13] A.V. Chichinadze, Theoretical and practical problems of thermal dynamics and simulation of the friction and wear of tribocouples, J. Friction Wear 30 (3) (2009) 199–215, https://doi.org/10.3103/S106836660903009X.
[14] F. Guo, Y. Yan, Y. Hong, Y. Li, Multiscale modeling: Prediction for thermophysical properties of needled carbon/carbon composite and evaluation of brake disk system, Mater. Today Commun. 22 (2020), https://doi.org/10.1016/j.mtcomm.2019.100685.
[15] A.A. Yevtushenko, P. Grzes, A. Adamowicz, The temperature mode of the carbon-carbon multi-disc brake in the view of the interrelations of its operating characteristics, Materials 13 (8) (2020) 1878, https://doi.org/10.3390/ma13081878.
[16] C. Meunier, J.G. Bauzin, N. Laraqi, A. Gapin, J.F. Diebold, Thermal characterization of the braking and cooling stages of an aircraft brake using identification techniques and a life-size experimental test bench, Int. J. Heat Mass Transfer 196 (2022), 123277, https://doi.org/10.1016/j.ijheatmasstransfer.2022.123277.
[17] L. Romualdi, N. Mancinelli, A. De Felice, S. Sorrentino, A new application of the extended Kalman filter to the estimation of roll angles of a motorcycle with inertial measurement unit, FME Trans. 48 (2) (2020) 255–265, https://doi.org/10.5937/fme2002255R.
[18] A.P. Teerhuis, S.T.H. Jansen, Motorcycle state estimation for lateral dynamics, Vehicle System Dynam. 50 (8) (2012) 1261–1276, https://doi.org/10.1080/00423114.2012.656 655.
[19] J. Dakhlallah, S. Glaser, S. Mammar, Y. Sebsadji, Tire-road forces estimation using extended Kalman filter and sideslip angle evaluation, in: Proceedings of the

American control conference, Westin Seattle Hotel, Seattle, WA, 2008, pp. 4597–4602.
[20] K. Bogdanski, M.C. Best, Kalman and particle filtering methods for full vehicle and tyre identification, Vehicle System Dynam. 56 (5) (2017) 769–790, https://doi.org/10.1080/00423114.2017.1337914.
[21] C.M. Martinez, E. Velenis, D. Tavernini, B. Gao and M. Wellers, Modelling and estimation of friction brake torque for a brake by wire system, 2014 IEEE International Electric Vehicle Conference (IEVC) (2014) 1-7. 10.1109/IEVC.2014.7056105.
[22] S. Sarkka, Bayesian Filtering and Smoothing, Cambridge University Press, Cambridge, 2013.
[23] M.C. Best, A.P. Newton, S. Tuplin, The identifying extended Kalman Filter: parametric system identification of a vehicle handling model, J. Multi-Body Dynam. 221 (1) (2007) 87–98, https://doi.org/10.1243/14644193JMBD68.